

Insight into glass transition of cellulose based on direct thermal processing after plasticization by ionic liquid

Jun Wu · Juan Bai · Zhigang Xue ·
Yonggui Liao · Xingping Zhou · Xiaolin Xie

Received: 7 July 2014 / Accepted: 6 November 2014 / Published online: 19 November 2014
© Springer Science+Business Media Dordrecht 2014

Abstract Ionic liquid plasticized cellulose (IPC) materials were prepared with microcrystalline cellulose (MCC) and 25–70 wt% 1-butyl-3-methylimidazolium chloride (BmimCl) by direct thermal processing. Their chemical, morphological and crystalline structures were characterized by Fourier transform infrared spectroscopy, scanning electron microscopy and X-ray diffraction, and their glass transition behaviors and mechanical properties were discussed. The results show there is no chemical reaction between cellulose and the ionic liquid. BmimCl only acts as a plasticizer to improve the thermal processability of MCC, the IPC materials show only one glass transition terrace and can be processed repeatedly. Based on the free volume transition and the percolation of continuous hydrogen bonding networks, the effects of free volume and

H-bonding interactions on the glass transition have been differentiated. Furthermore, the phase diagram with four regions has been plotted for IPC materials, which is useful to optimize the thermal processing and modulate the properties of cellulose materials.

Keywords Cellulose · Ionic liquid · Plasticization · Thermal processing · Hydrogen bonding · Glass transition

Abbreviations

MCC	Microcrystalline cellulose
T_g	Glass transition temperature
IPC	Ionic liquid plasticized cellulose
FT-IR	Fourier transform infrared spectroscopy
DSC	Differential scanning calorimetry
XRD	X-ray diffraction
SEM	Scanning electron microscopy
G-T/K-B equation	Gordon-Taylor/Kelley-Bueche equation

J. Wu · J. Bai · Z. Xue · Y. Liao (✉) · X. Zhou ·
X. Xie (✉)

Key Laboratory for Large-Format Battery Materials and System, Ministry of Education, School of Chemistry and Chemical Engineering, Huazhong University of Science and Technology, Wuhan 430074, China
e-mail: ygliao@mail.hust.edu.cn

X. Xie
e-mail: xlxie@mail.hust.edu.cn

Y. Liao · X. Xie
State Key Laboratory of Materials Processing and Die and Mould Technology, School of Chemistry and Chemical Engineering, Huazhong University of Science and Technology, Wuhan 430074, China

Introduction

Cellulose, a linear polysaccharide with a β -(1 → 4)-linked D-glucose unit and the most abundant natural polymer on earth from green plants and some bacteria (Wang et al. 2012), has been widely applied in

packaging, durable goods, electronics, biomedical uses, etc. (Gericke et al. 2013; Reddy et al. 2013) for its renewability, biocompatibility and outstanding mechanical properties (Diddens et al. 2008). Due to the numerous inter- and intramolecular hydrogen bonds (H-bonds) (Pinkert et al. 2009) and amphiphilicity of repeat units (Lindman et al. 2010; Medronho et al. 2012), cellulose can neither dissolve in common solvents nor melt at elevated temperature even above the decomposition temperature (Calahorra et al. 1989), which makes this fantastic material difficult to process. Although chemical modifications such as esterification and etherification provide processable derivatives (Klemm et al. 2005), direct utilization of natural cellulose remains a big challenge. The development of efficient solvent systems has led to breakthrough progress in wet processing (Johnson 1969; Dupont 2003; Cai and Zhang 2005; Swatloski et al. 2002), but thermal processing methods, which can produce bulky materials with various shapes conveniently and efficiently, are preferred in the modern plastics industry. Unfortunately, only limited progress has been achieved. Schroeter and Felix (2005) fabricated a transparent cellulose disk with a diameter of 3 mm and thickness of 20 μm via strong mechanical shear, high pressure and large-dose laser radiation. By means of back pressure-equal channel angular press (BP-ECAP) technology, Zhang et al. (2012) successfully prepared bulky plastics with a storage modulus up to 1.0 GPa from cellulose powders under an ultrahigh pressure of above 100 MPa. However, both technologies need specific instruments and are highly inefficient for industrial applications.

According to the reptation theory proposed by Edwards and de Gennes, the motion of a whole macromolecular chain leading to flowing comprises the segmental motion, which is directly related to the glass transition behavior. Since the cellulose starts to oxidize and decompose at ~ 473 K (Mamleev et al. 2007), and there are small variations in the heat capacity during the glass transition of cellulose (Szcześniak et al. 2008), it is not a trivial task to measure the glass transition temperature (T_g) of dry cellulose directly. Recently, the experimental T_g values of dehydrated cellulose and ball-milled dry cellulose were reported to be 357 and 433 K, respectively, by differential scanning calorimetry (DSC) and dynamic mechanical analysis (DMA) (Roig et al. 2011; Paes et al. 2010). To filter out the thermal

decomposition, Kim et al. (2013) used a step scan mode DSC to measure the T_g of 573 K for cellulose films. Obviously, the above values are discrepant and difficult to understand. From the predictive relationship between T_g and solvent content in solvent-containing samples, T_g of pure cellulose has been extrapolated to be 493–523 K (Szcześniak et al. 2008; Bizot et al. 1997), which is consistent with the simulation result through specific volume (Chen et al. 2004). Setting the T_g of pure cellulose as a generally accepted value of ~ 500 K, the relationship between T_g and water content has been successfully described by the Gordon-Taylor/Kelley-Bueche (G-T/K-B) equation (Hancock and Zografis 1994), Kaelbe's approach (Szcześniak et al. 2008) and Couchman's equation (Paes et al. 2010). However, the assumption of "no specific interactions between components" in the G-T/K-B equation based on free volume could not be satisfied because of the existence of powerful H-bonding networks (Mazeau and Heux 2003). It is well known that strong H-bonds exist in cellulose, and their confinement on molecular chain motion leads to a high T_g . Though the intermolecular H-bonds in hydrated cellulose can be interrupted by water, the effect is limited, especially at low water content. Experimental T_g of cellulose with 5.3 and 7 % water content shows a discrepancy from the prediction of Kaelbe's approach, which is attributed to the strong H-bonding interactions between the chains (Szcześniak et al. 2008); that is, the effect of on T_g is considerable, but it cannot be reflected in the free volume-based equations. Therefore, to differentiate the effects of H-bonding and free volume on the T_g of cellulose is urgently needed for understanding the basics of glass transition behavior.

Ionic liquids have been found to be effective plasticizers for polymers such as poly(methyl methacrylate) (Scott et al. 2002) and poly(vinyl chloride) (Choi et al. 2011, 2014). Their influences on the thermal processability and the relationship of dissolution and gelatinization of starch were also reported (Sankri et al. 2010; Mateyawa et al. 2013). In this work, an ionic liquid of 1-butyl-3-methylimidazolium chloride (BmimCl) was used as a plasticizer to prepare ionic liquid plasticized cellulose (IPC) materials. Due to the aggressive ability to break H-bonds and crystal structures of cellulose, BmimCl is better than water to improve the mobility of cellulose chains. Furthermore, its nonvolatility broadens the processing temperature

window, which is helpful to the thermal processability of cellulose. IPC materials with 25–70 wt% BmimCl were prepared using direct thermal processing, and their glass transition mechanism was investigated via a linear form of the G-T/K-B equation and a prediction about the percolation transition of H-bonding networks. Finally, the contributions of free volume and H-bonding networks to the glass transition of cellulose were discussed.

Experimental section

Materials and sample preparation

Microcrystalline cellulose (MCC) was purchased from Sinopharm Chemical Reagent Co., Ltd. (Shanghai, China) with a crystallinity of 66.9 %. About 1.5 wt% moisture was confirmed by thermogravimetry analysis and removed at 125 °C under vacuum for 48 h. 1-Butyl-3-methylimidazolium chloride (BmimCl, 99 %) was purchased from Dibo reagent Co., Ltd. (Shanghai, China) and used as received.

BmimCl plasticized cellulose (IPC) materials with 25–70 wt% BmimCl were first hot compounded on a ZG-76 two-roll mill (Zhengcong Mechanical and Electrical Equipment Technology Co., Ltd., Dongguan, China) at 130 °C for 15 min with the two roll speeds set to 8.6 and 10 rpm. Then, they were calendared into film samples with a thickness of about 0.25 mm for FT-IR, DSC and XRD measurements. The thick film samples (~1 mm) with 30–50 wt% BmimCl for mechanical tests and fracture morphology measurement were compression-molded on a PL-6170C plate vulcanizing machine (Bolon Precision Testing Machines Co., Ltd., Dongguan, China) under 130 °C and 10 MPa for 5 min, with a 3-min preheating period. For evaluating the thermal processability, the IPC materials with 40 wt% of BmimCl were also injection-molded using a TY-200 vertical injection machine (Tayu Machinery Co., Ltd., Hangzhou, China). The barrel-zone temperatures of the injection-molding machine were set at 160, 155, 155, 150 and 150 °C, the injection pressure and rate were 13 MPa and 10 cm³/s, and the cooling time was set at 60 s for sufficient solidification of samples. To check the thermal reprocessability of the IPC materials, the sample with 40 wt% of BmimCl was prepared for five

cycles of repeated thermoprocessing on the two-roll mill and cooled to room temperature.

All samples were sealed immediately and naturally cooled to room temperature after processing and kept in a drier with argon before use.

Measurements

Fourier transform infrared (FT-IR) analysis was conducted on a spectrometer (Bruker V70, Germany) with a reflectance accessory. A scan range from 4,000 to 600 cm⁻¹ was chosen with a resolution of 4 cm⁻¹, and 16 scans were performed for each sample. Tensile tests of IPC with a dimension of about 10 × 25 × 1 mm³ were conducted on a CMT4104 universal testing machine (SANS, Shenzhen, China) with 25 mm gauge length and a cross-head rate of 10 mm/min. At least six samples of each IPC were tested, from which the mean values and standard deviations were calculated. Field emission scanning electron microscopy (SEM, Sirion 200, The Netherlands) was used to determine the morphology of the fracture surface of IPC materials. A thin layer of platinum was sputtered onto the samples after breaking off in liquid nitrogen prior to SEM imaging. Wide-angle X-ray diffraction (XRD) analysis was carried out on an X-ray diffractometer (X'Pert PRO, The Netherlands) by a reflection method using a Cu K α target at 40 kV, and the diffraction angle (2θ) ranged from 5° to 60°. Crystallinity was calculated through the ratio of the area of crystalline peaks to total area. The thermal analyses of IPC materials were conducted with a differential scanning calorimeter (DSC, Q2000, TA Instruments) at a rate of 20 K/min in nitrogen. About 10 mg of IPC materials was subjected to an initial temperature ramp to 433 K and kept for 15 min to completely remove any residual absorbed water and then ramped down to 193 K. Eventually, the IPC materials were heated to 393 K. To clarify the transition terrace, the temperature ranges for IPC materials and pure BmimCl were given in the DSC curves from 223 to 333 and 213 to 333 K, respectively. The T_g of IPC materials was determined by the deflection point of the second heat flow curves. The T_g for pure BmimCl was 225 K according to the reference (Yamamuro et al. 2006) and also confirmed in this work.

Results and discussion

Thermal processability, mechanical properties, morphology and formation mechanism of IPC materials

In general, the processability of IPC materials increases with BmimCl content. IPC materials with BmimCl content <25 wt% were too brittle to process, while IPC materials with BmimCl content more than 70 wt% were not geometrically stable. Therefore, IPC materials with 25–70 wt% BmimCl were successfully fabricated through calendaring, and thick film samples (~1 mm) with 30–50 wt% BmimCl were compression molded. Figure 1a and b shows typical photos of the calendared film and the hot-compressed plate of IPC with 40 wt% of BmimCl. It can be seen that the calendared film with 0.25 mm thickness is uniform and partially transparent, and the hot-compressed plate with dimensions of $70 \times 50 \times 1 \text{ mm}^3$ is successfully fabricated. Further, typical impact ($80 \times 10 \times 4 \text{ mm}^3$) and tensile ($75 \times 10 \times 2 \text{ mm}^3$) samples without surface defects can be injection molded, as shown in Fig. 1c. These indicate that the IPC materials have sufficient processability for direct thermal processing.

FT-IR spectra of BmimCl, MCC and IPC with 30 wt% BmimCl are shown in Fig. 2. For BmimCl, absorption peaks at 3,095, 2,865, 1,563 and $1,463 \text{ cm}^{-1}$ are attributed to stretching vibrations of unsaturated C–H, saturated C–H, C–N and C=C in the imidazole cation, respectively. For MCC, the broad absorption peak from 3,540 to $3,180 \text{ cm}^{-1}$ is attributed to O–H stretching vibrations of various forms of free and hydrogen-bonded hydroxyl groups. The absorption peak ranging from 1,160 to $1,030 \text{ cm}^{-1}$ is

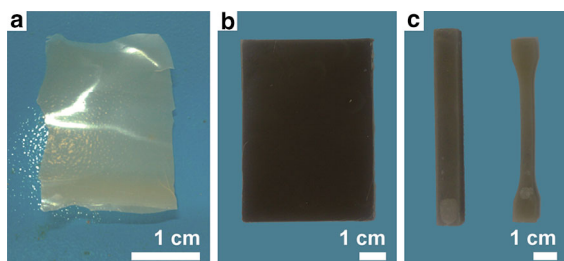


Fig. 1 Photographs of IPC with 40 wt% BmimCl processed by calendaring (a), compression molding (b) and injection molding (c)

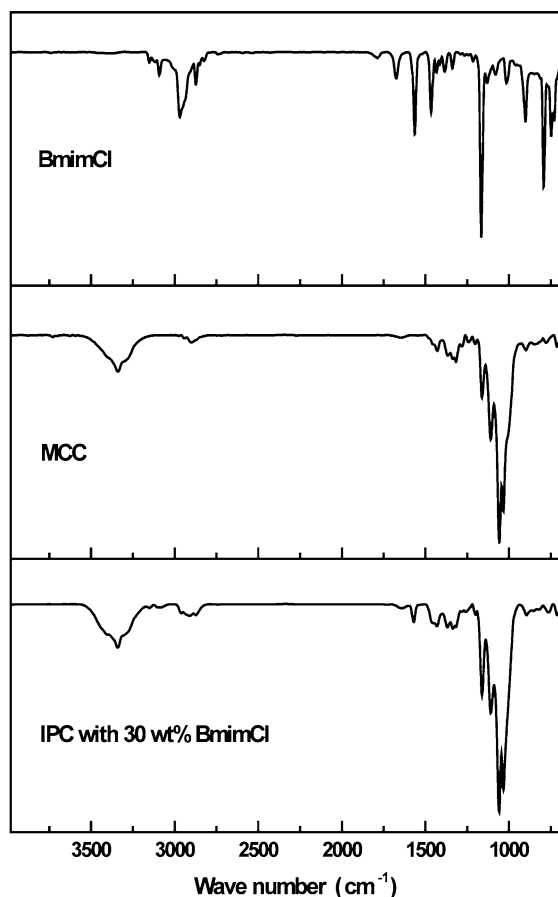


Fig. 2 FT-IR spectra of BmimCl, MCC and IPC with 30 wt% BmimCl

attributed to C–OH stretching vibrations of primary and secondary hydroxyl, and peaks at 1,430 and $1,315 \text{ cm}^{-1}$ are contributed by scissor bending and twisting of $-\text{CH}_2$ in the main chain. Compared with MCC and pure BmimCl, IPC with 30 wt% BmimCl shows no new absorption peaks. This is because BmimCl is a nonderivative solvent for cellulose (Swatloski et al. 2002), there is no chemical reaction between cellulose and the ionic liquid, BmimCl only acts as a plasticizer to improve the processability of MCC, and the IPC materials are stable during thermal processing.

The mechanical properties of IPC materials with 30–50 wt% BmimCl are listed in Table 1. Due to the plasticization effect of BmimCl, the tensile strength and Young's modulus decrease almost one order of magnitude as the BmimCl content increases from 30 to 50 wt%, i.e., from 200.7 and 8.3 MPa to 32.0 and

Table 1 Mechanical properties of IPC materials with different contents of BmimCl and IPC with 40 wt% of BmimCl after five reprocessed times (denoted as 40 %-5R)

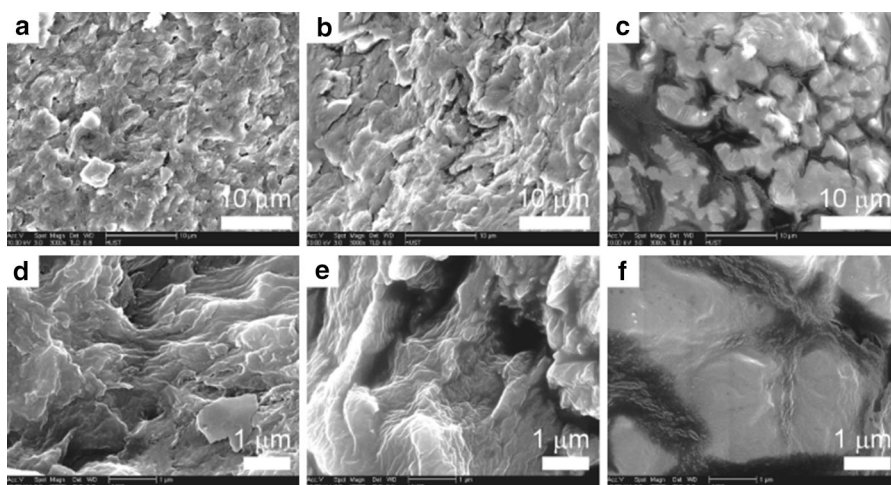
BmimCl content (wt%)	Young's modulus (MPa)	Tensile strength (MPa)	Elongation at break (%)
30 %	200.7 ± 9.8	8.3 ± 0.9	6.4 ± 0.9
40 %	66.7 ± 3.3	3.0 ± 0.2	14.2 ± 1.7
50 %	32.0 ± 1.6	1.0 ± 0.1	9.4 ± 3.5
40 %-5R	68.1 ± 15.4	3.1 ± 0.2	13.6 ± 2.2

1.0 MPa, respectively. Although these data are far from those for native cellulose (138 and 13–17 GPa for cellulose I, 88 and 9 GPa for cellulose II, 10 GPa and 800 MPa for amorphous cellulose) (Huber et al. 2011; Nishino et al. 1995), these materials show a potential for making bulk materials, especially with a low BmimCl content. Meanwhile, their elongation at break increases from 6.4 to 14.2 %, which is indicative of a little enhancement of toughness. It is worth noted that the IPC with 40 wt% BmimCl had the highest elongation at break. With the addition of BmimCl, the plasticization effect increases the free volume and weakens the H-bonds in the IPC materials, leading to an increase in elongation at break. However, excess plasticizer acts as an activation cell for crack formation (Jacobsen and Fritz 1999), which makes the IPC easier to break and results in a decrease in elongation.

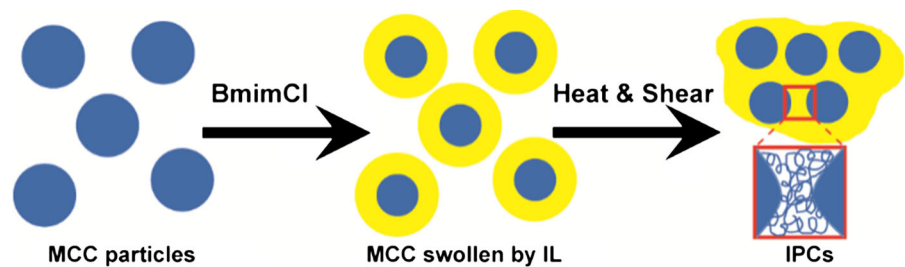
The fracture surface morphologies of IPC materials are shown in Fig. 3. For the IPC with 30 wt% BmimCl as shown in Fig. 3a and d, the boundaries of the

spliced MCC domains are sharp and clear. When the BmimCl content is increased to 40 wt%, the plasticized MCC domains with obtuse and fuzzy boundaries can be observed (Fig. 3b and e). For IPC with 50 wt% BmimCl (Fig. 3c, f), the MCC domains are merged together by the swollen MCC boundaries, which form the continuous matrix. Thus, a formation mechanism of IPC during thermal compression can be illustrated in Scheme 1. As a good solvent for cellulose, BmimCl disaggregates MCC particles from the outside, forming MCC domains with swollen amorphous boundaries. The chain mobility in the outside swollen boundaries is enhanced by the interruption of H-bonds and increase in free volume. The disentanglement and sliding of the cellulose chains in the swollen boundaries occur under heating and shearing. As a result, the effective interchain penetration of the cellulose chains in the amorphous boundaries merges individual MCC domains. With increasing BmimCl content, the mobility of cellulose chains is further enhanced, leading to improved processibility.

Based on the plasticization effect of ILs, this is the first report on direct thermal processing of natural cellulose using industrial equipment including a two-roll mill, plate vulcanizing machine and injection machine. More interestingly, the IPC materials can be processed repeatedly. Due to the oxidation and decomposition of cellulose, the hue of IPC materials became a bit darker with increased reprocessed times. However, the mechanical properties of IPC materials remained good after reprocessing five times. Hence, from Table 1, it can be seen that the IPC with 40 wt%

Fig. 3 SEM images of cryofractured IPC materials with BmimCl content of 30 wt% (a, d); 40 wt% (b, e); 50 wt% (c, f)

Scheme 1 Formation mechanism of IPC materials during thermal processing



BmimCl retains a Young's modulus of 68.1 MPa, tensile strength of 3.1 MPa and elongation of 13.6 %. Recently, Wang et al. (2013) prepared a hydrogel with NaOH/urea aqueous solution as solvent and fabricated the cellulose plastic with excellent mechanical performance under 90–190 °C and pressure of 60 MPa by thermal compression accompanied by removal of water. It is clear that this cellulose plastic cannot be reprocessed, which is different from our IPC materials.

Crystalline structure of IPC materials

The normalized XRD spectra of MCC and IPC materials with different BmimCl contents are shown in Fig. 4. All IPC materials have the characteristic peaks of cellulose I crystal in natural cellulose at 14.8°, 16.2° and 22.7° for (1 $\bar{1}$ 0) (110) and (200) planes, respectively (Nishiyama et al. 2002; French 2014). Also, a clear peak at 20.6° for (012) and (102) planes in cellulose I α is observed in MCC and IPC materials with low BmimCl content, and no

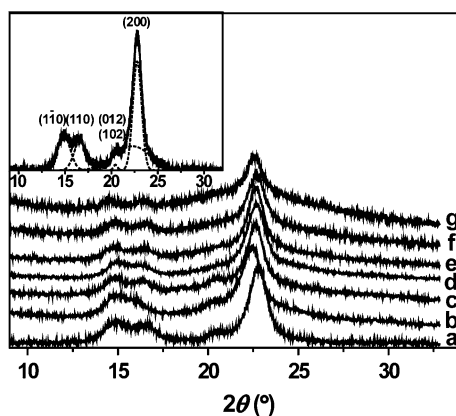


Fig. 4 Normalized XRD spectra of MCC (a) and IPC materials with BmimCl content of 30 wt% (b), 40 wt% (c), 40 wt% reprocessed five times (d), 50 wt% (e), 60 wt% (f) and 70 % (g), respectively. *Inset* is the peak fitting of MCC

characteristic peaks of cellulose II crystal exist in regenerated cellulose (Duchemin et al. 2009; Han and Yan 2010). Although having a melting point of 68 °C, BmimCl is a liquid once heated at high temperature and cooled to room temperature due to its strong tendency for supercooling (Galiński et al. 2006). Also, the XRD curves of IPC materials only show the characteristic peaks of cellulose I even at high BmimCl contents up to 70 wt%. Thus, the crystalline peaks of the XRD curves are attributed to the cellulose crystalline phases in the IPC materials. As shown in the inset of Fig. 4, the amorphous and crystalline phases in MCC and IPC materials are distinguished quantitatively via the peak fitting technique, and the crystallinity of cellulose (φ) is achieved. Figure 5 shows the crystallinity of MCC and IPC materials with different BmimCl contents. The crystallinity decreases almost linearly with increasing BmimCl content. With a fixed intercept of 66.9 % (crystallinity of MCC), the BmimCl content dependence of crystallinity can be fitted by the equation below:

$$\varphi = -0.557c + 0.669 \quad (1)$$

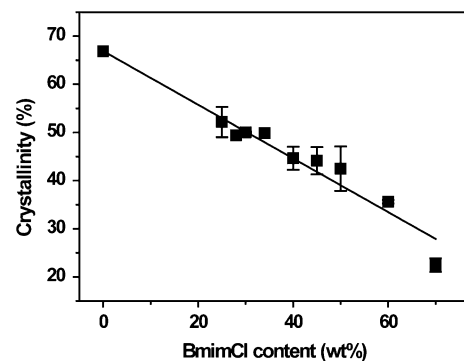


Fig. 5 Crystallinity of IPC materials as a function of BmimCl content

Even at high BmimCl content up to 70 wt%, the IPC still retains a crystallinity of 23.5 %. It is noted that the dependence of BmimCl on the crystallinity of cellulose is different from the independence of water (Hancock and Zografí 1994; Szcześniak et al. 2008), indicating the stronger plasticization effect of ionic liquid on the processability of cellulose. Furthermore, the regeneration of cellulose II did not occur in the IPC materials during thermal processing, while the recrystallization to cellulose I from amorphous phases might happen as reported by Schall (Samayam et al. 2011). Additionally, the crystallinities of IPC with 40 wt% BmimCl are 44.6 and 38.8 % before and after reprocessing five times. Like in the discussion of the hue change during reprocessing, this decrease is attributed to the oxidation and decomposition of the cellulose.

Glass transition behavior of IPC materials

The DSC curves of MCC and IPC materials with different BmimCl contents are shown in Fig. 6. For MCC, no thermal transition signal can be observed in the experimental temperature range. For pure BmimCl, a T_g of 227.0 K is in good agreement with the 225.0 K °C reported by Yamamuro et al. (2006). The IPC with 30 wt% BmimCl shows a tiny glass transition around 281.7 K. With increasing BmimCl content, the transition shifts to lower temperature, suggesting that the cellulose segments move more easily because of the plasticization effect of BmimCl.

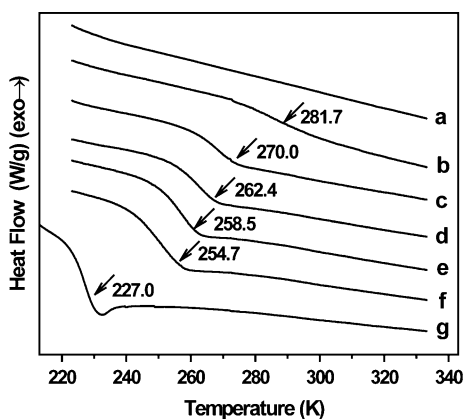


Fig. 6 DSC curves of MCC (a), IPC materials with BmimCl content of 30 wt% (b), 40 wt% (c), 50 wt% (d), 60 wt% (e), 70 wt% (f) and pure BmimCl (g)

The change of heat capacity of IPC materials during glass transition also becomes greater, which makes the transition terrace clearer. All IPC materials show only one transition terrace, which indicates that MCC and BmimCl are compatible (Hancock and Zografí 1994). Interestingly, the transitions are also observed in cooling runs and subsequent cycles. The reversible glass transition behavior in these IPC materials is different from that in wet-processed samples (Shi et al. 2011).

The G-T/K-B equation (Gordon and Taylor 1952) (Eq. 2) simplified by the Samba-Boyer rule (Eq. 3) is usually used to describe the glass transition temperature ($T_{g,m}$) in compatible amorphous polymer blends or plasticized systems (Hancock and Zografí 1994; Schneider 1989).

$$T_{g,m} = \frac{w_p \cdot T_{g,p} + K \cdot w_c \cdot T_{g,c}}{w_p + K \cdot w_c}; \quad K = \frac{\rho_p \cdot \Delta\alpha_c}{\rho_c \cdot \Delta\alpha_p} \quad (2)$$

$$\Delta\alpha \cdot T_g \approx 0.113; \quad K = \frac{\rho_p \cdot T_{g,p}}{\rho_c \cdot T_{g,c}} \quad (3)$$

where $T_{g,p}$ and $T_{g,c}$ are the glass transition temperatures of the plasticizer and pure polymer, i.e., cellulose in this work; w_p and w_c represent the mass fraction of each component. K is a constant decided by the density (ρ) and the change of thermal expansivity ($\Delta\alpha$) of components at T_g . Herein, ρ_p and ρ_c are 1.08 and 1.54 g/cm³, respectively.

However, the glass transition behavior of a semi-crystalline polymer originates from the amorphous region in which the plasticizer is located (Zografí et al. 1984). Therefore, w_p should be recalculated with the apparent mass fraction of the plasticizer (c), the crystallinity φ of cellulose, which can be written as

$$w_p = \frac{m_p}{m_p + m_c \cdot (1 - \varphi)} = \frac{c}{1 - \varphi + c\varphi} \quad (4)$$

where m_p and m_c represent the masses of plasticizer and cellulose, respectively.

In addition, the strong intermolecular H-bonding interaction between MCC and BmimCl gradually destroyed the crystalline regions of cellulose with increasing BmimCl content, so the crystallinity of cellulose in IPC materials should be taken as a variable parameter.

As mentioned above, the G-T/K-B equation is based on the free volume assumption, and the existence of H-bonds leads to a high T_g . Compared

to water, BmimCl has a greater ability to interrupt H-bonds in cellulose and a higher actual content in the plasticized system; thus, a weaker H-bonding level gives rise to a lower T_g in IPC materials. Since the strength of the H-bonds depends on the BmimCl content, the continuous H-bonding networks will be broken at a critical BmimCl content. That is, there is a percolation transition for the continuous H-bonding networks. Therefore, it is not reasonable to take all data equally in a single fitting line; otherwise, the result would be inaccurate with systematic error caused by the H-bonding interactions. To differentiate the effects of free volume and H-bonding interactions on T_g , a linear form of the G–T/K–B equation is proposed for further investigation. Rather than an intangible fitting, which considers every datum equally, a linear form is a more reasonable method to determine whether the experimental data are consistent with the physical meaning or not. Consequently, the influence of H-bonding interactions on T_g can be visualized.

Through a mathematical transformation of the classic G–T/K–B equation, a linear correction form with the apparent content and crystallinity can be written as:

$$\frac{T_{g,p}}{T_{g,m}} = b \cdot \left[\frac{\rho_p \cdot (T_{g,p} - T_{g,c})}{T_{g,c}} \cdot \frac{1}{\rho_p + z} + 1 \right] \quad (5)$$

$$z = \frac{w_p \cdot \rho_c}{1 - w_p} = \frac{c \cdot \rho_c}{(1 - c) \cdot (1 - \phi)} \quad (6)$$

where b is a correction factor with respect to the deviation from the ideal G–T/K–B correlation. The closer the intercept b is to 1, the better the experimental data obey the theoretical equation.

Experimental data points are plotted in the new coordinate system of $T_{g,p}/T_{g,m}$ versus $1/(\rho_p + z)$ in Fig. 7. Obviously, the experimental data with $1/(\rho_p + z)$ from 0.174 to 0.414 (w_p from 74.9 to 55.2 wt%; c from 70 to 30 wt%) in the left part of the plot have a good linear relationship. However, the experimental data for the IPC materials with $1/(\rho_p + z)$ more than 0.414 ($w_p < 55.2$ wt%; $c < 30$ wt%) in the bottom right part of Fig. 7 clearly deviate negatively from the fitting line. This deviation is attributed to the interactions of continuous H-bonding networks in IPC materials. The onset of deviation, 0.414 of $1/(\rho_p + z)$ (w_p is 55.2 wt%; c is 30 wt%), is a critical content

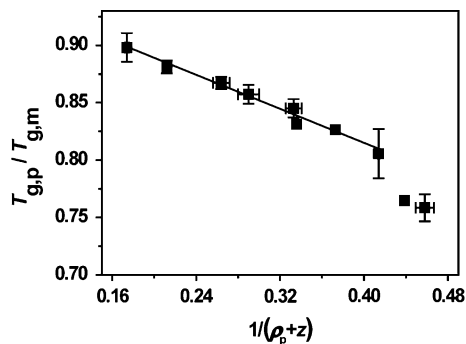


Fig. 7 Relationship between $T_{g,p}/T_{g,m}$ and $1/(\rho_p + z)$ for the linear correction G–T/K–B equation

where the transition of free volume and percolation of H-bonding networks happen simultaneously. Below the critical BmimCl content, the H-bonding interaction in IPC materials is still strong enough to form continuous networks and restricts the segmental motion of cellulose even if the free volume provides enough space for the segmental relaxation. Actually, $T_{g,m}$ is the dissociation temperature of the H-bonding networks. By contrast, above the critical BmimCl content, the temperature for destroying the continuous H-bonding networks is lower than that for the segmental relaxation from the free volume contribution. Thus, $T_{g,m}$ matches the prediction of the G–T/K–B equation well.

The left part of the plot in Fig. 7 can be expressed as

$$\frac{T_{g,p}}{T_{g,m}} = 0.963 \times \left(-0.385 \times \frac{1}{\rho_p + z} + 1 \right) \quad (7)$$

As expected, the intercept b of 0.963 is very close to unity. From the slope of the straight line, a glass transition temperature of pure cellulose, $T_{g,c}$, can be estimated as 353 K, which is ascribed to the contribution of free volume. This value is close to 357 K of pure dehydrated cellulose (Roig et al. 2011).

For comparison, a direct fitting curve of all IPC materials (dashed curve) and the curve fitted by our method using partial IPC materials with w_p from 74.9 to 55.2 wt% (c from 70 to 30 wt%, solid curve) are shown in Fig. 8. Without the interruption of data points with continuous H-bonding networks, the solid curve fits the data points with high BmimCl contents better than the dashed curve, which is supported by the higher correlation coefficient R . That is, $R^2 = 0.96$ versus $R^2 = 0.93$.

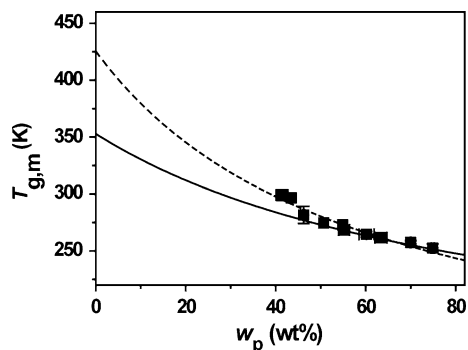


Fig. 8 Direct fitting curve of samples with all BmimCl contents (*dashed line*) and the curve fitted using samples with BmimCl from 30 to 70 wt% contents (*solid line*)

Up to now, the quantitative relationship between the dissociation temperature of H-bonding networks (T_H) and the H-bond density is still unclear. Recently, Brovchenko et al. (2011) found that the dissociation temperature of H-bonding networks depended linearly on the average number of H-bonds by computer simulation. Therefore, the relationship between T_H and w_p can be ratiocinated to be linear. Since IPC materials with $c < 25$ wt% ($w_p < 41.4$ wt%) are difficult to prepare, we only achieved three points below the critical value to roughly forecast the dependence of w_p on T_H . The linear fitting result is shown in Fig. 9, which can be expressed as:

$$T_H = -373.7w_p + 455.8 \quad (8)$$

The intercept of about 456 K is considered to be T_H of pure cellulose, i.e., the actual T_g of cellulose.

With the two functional relations in Eqs. 7 and 8, a phase diagram of apparent $T_{g,m}$ as a function of w_p is

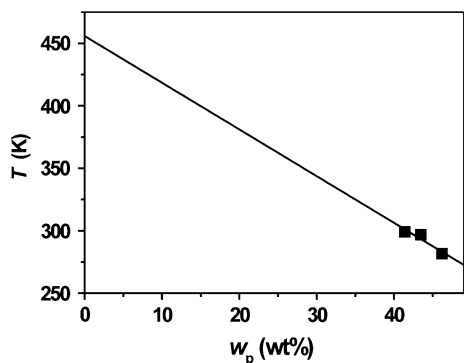


Fig. 9 Relationship between the dissociating temperature of continuous H-bonding networks and w_p

clearly defined in Fig. 10a. For better perception and easier application, the phase diagram is transformed with the x -axis of c , as shown in Fig. 10b. According to the basics of segmental mobility, the apparent $T_{g,m}$ of IPC materials is decided by the dominant contribution of either the free volume or the specific interaction of continuous H-bonding networks. Based on the contribution of the two factors on glass transition, the phase diagram can be divided into four regions: (I) the rubber state with sufficient free volume and without H-bonding networks, (II) glass state without sufficient free volume and H-bonding networks, (III) glass state with insufficient free volume and continuous H-bonding networks, and (IV) glass

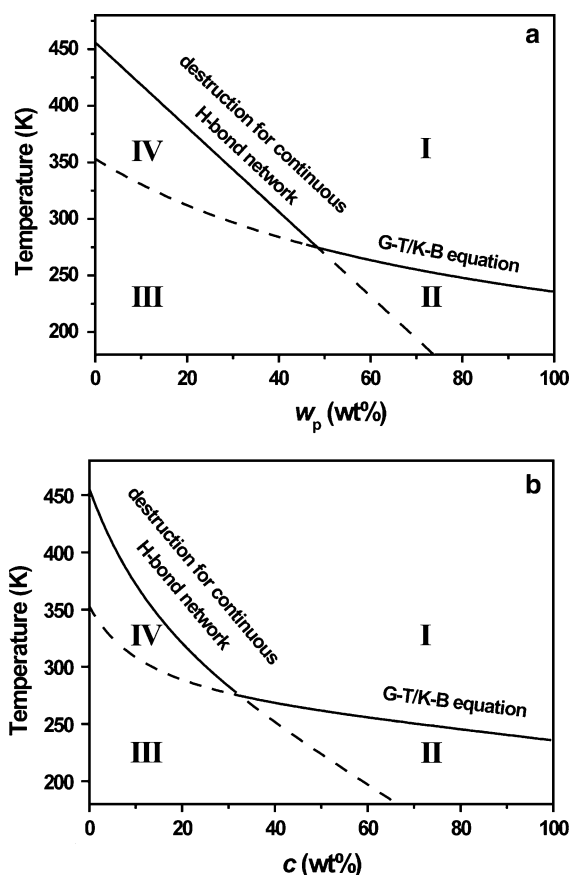


Fig. 10 Phase diagrams of apparent $T_{g,m}$ as a function of w_p (a) and c (b). The four regions in the diagrams represent: (I) rubber state with sufficient free volume and without H-bonding networks, (II) glass state without sufficient free volume and H-bonding networks, (III) glass state with insufficient free volume and continuous H-bonding networks, and (IV) glass state with sufficient free volume and continuous H-bonding networks

state with sufficient free volume and continuous H-bonding networks. For pure cellulose, the free volume provides enough space for segmental relaxation at 353 K, while the continuous H-bonding networks are destructed at 456 K. By adding BmimCl, both transition temperatures decrease, but the latter one decreases faster. The apparent T_g is gradually close to the predicted value from the G-T/K-B equation, and finally they coincide. The intersection at w_p of 46.2 wt% (c of 30 wt%) with the temperature of about 281 K for both transitions indicates a mechanism transform from the H-bonding network control to the free volume control in the glass transition behavior. Further, region (I) is the thermal processing window in which the high temperature and sufficient plasticizer break the continuous H-bonding networks and provide sufficient free volume, so that the enhanced segmental mobility is useful for processing the IPC materials. Besides, the cellulose chains are restricted the most in region (III) by the continuous H-bonding networks and insufficient free volume, thereby imparting the materials with excellent mechanical properties and stability. From the phase diagram, we can optimize the thermal processing and modulate the properties of the cellulose materials by adjusting the temperature and plasticizer content synergistically.

Conclusion

IPC materials with 25–70 wt% BmimCl have been successfully prepared by thermal processing. There is no chemical reaction between cellulose and the ionic liquid, BmimCl only acts as a plasticizer to improve the thermal processability of MCC, and the IPC materials can be processed repeatedly. Due to the plasticization effect of BminCl, the tensile strength and Young's modulus of IPC materials decrease with increasing BminCl content, and the IPC with 40 wt% BmimCl has the highest elongation at break. Additionally, the crystallinity of cellulose in IPC materials decreases linearly with BmimCl content. Even at high BmimCl contents up to 70 wt%, the IPC still retains a crystallinity of 23.5 % compared with 66.9 % of MCC. Interestingly, all IPC materials show only one glass transition, and their $T_{g,m}$ values decrease with BmimCl content.

A linearized form of the G-T/K-B equation containing apparent BmimCl content (c) and crystallinity of cellulose (φ) has differentiated the effects of free volume and H-bonding interactions on T_g . The proposed 353 and 456 K are related to the transitions of free volume and percolation of H-bonding networks in cellulose, respectively. Subsequently, the phase diagram with four regions has been plotted for the IPC materials, which is useful for the optimization of thermal processing and modulation of the properties of the cellulose materials. Further, the phenomenological method used in this work is expected to apply to other polymer systems with H-bonding interactions.

Acknowledgments The authors acknowledge the financial support of the National Basic Research Program of China (973 Program, 2012CB025903), the National Natural Science Foundation of China (51210004, 51373060) and the Chinese Ministry of Education (NCET-11-0174). We also thank the Analytical and Testing Center of HUST for SEM and XRD measurements.

References

- Bizot H, LeBail P, Leroux B, Davy J, Roger P, Buleon A (1997) Calorimetric evaluation of the glass transition in hydrated, linear and branched polyanhydroglucose compounds. *Carbohydr Polym* 32:33–50
- Brovchenko I, Andrews MN, Oleinikova A (2011) Thermal stability of the hydrogen-bonded water network in the hydration shell of islet amyloid polypeptide. *J Phys Condens Matter* 23:155105
- Cai J, Zhang L (2005) Rapid dissolution of cellulose in LiOH/urea and NaOH/urea aqueous solutions. *Macromol Biosci* 5:539–548
- Calahorra ME, Cortázar M, Eguiazábal JI, Guzmán GM (1989) Thermogravimetric analysis of cellulose: effect of the molecular weight on thermal decomposition. *J Appl Polym Sci* 37:3305–3314
- Chen W, Lickfield GC, Yang CQ (2004) Molecular modeling of cellulose in amorphous state. Part I: model building and plastic deformation study. *Polymer* 45:1063–1071
- Choi SY, Rodriguez H, Mirjafari A, Gilpin DF, McGrath S, Malcolm KR, Tunney MM, Rogers RD, McNally T (2011) Dual functional ionic liquids as plasticisers and antimicrobial agents for medical polymers. *Green Chem* 13:1527–1535
- Choi SY, Rodriguez H, Gunaratne HQN, Puga AV, Gilpin D, McGrath S, Vyle JS, Tunney MM, Rogers RD, McNally T (2014) Dual functional ionic liquids as antimicrobials and plasticisers for medical grade PVCs. *RSC Adv* 4:8567–8581
- Diddens I, Murphy B, Krisch M, Müller M (2008) Anisotropic elastic properties of cellulose measured using inelastic X-ray scattering. *Macromolecules* 41:9755–9759

- Duchemin BJC, Newman RH, Staiger MP (2009) Structure–property relationship of all-cellulose composites. *Compos Sci Technol* 69:1225–1230
- Dupont A-L (2003) Cellulose in lithium chloride/*N,N*-dimethylacetamide, optimisation of a dissolution method using paper substrates and stability of the solutions. *Polymer* 44:4117–4126
- French AD (2014) Idealized powder diffraction patterns for cellulose polymorphs. *Cellulose* 21:885–896
- Galiński M, Lewandowski A, Stępnik I (2006) Ionic liquids as electrolytes. *Electrochim Acta* 51:5567–5580
- Gericke M, Trygg J, Fardim P (2013) Functional cellulose beads: preparation, characterization, and applications. *Chem Rev* 113:4812–4836
- Gordon M, Taylor JS (1952) Ideal copolymers and the second-order transitions of synthetic rubbers. I. Non-crystalline copolymers. *J Appl Chem* 2:493–500
- Han D, Yan L (2010) Preparation of all-cellulose composite by selective dissolving of cellulose surface in PEG/NaOH aqueous solution. *Carbohydr Polym* 79:614–619
- Hancock B, Zograf G (1994) The relationship between the glass transition temperature and the water content of amorphous pharmaceutical solids. *Pharm Res* 11:471–477
- Huber T, Müssig J, Curnow O, Pang S, Bickerton S, Staiger MP (2011) A critical review of all-cellulose composites. *J Mater Sci* 47:1171–1186
- Jacobsen S, Fritz HG (1999) Plasticizing polylactide—the effect of different plasticizers on the mechanical properties. *Polym Eng Sci* 39:1303–1310
- Johnson DL (1969) Compounds dissolved in cyclic amine oxides. US Patent 3,447,939
- Kim J-W, Park S, Harper DP, Rials TG (2013) Structure and thermomechanical properties of stretched cellulose films. *J Appl Polym Sci* 128:181–187
- Klemm D, Heublein B, Fink H-P, Bohn A (2005) Cellulose: fascinating biopolymer and sustainable raw material. *Angew Chem Int Ed* 44:3358–3393
- Lindman B, Karlström G, Stigsson L (2010) On the mechanism of dissolution of cellulose. *J Mol Liq* 156:76–81
- Mamleev V, Bourbigot S, Yvon J (2007) Kinetic analysis of the thermal decomposition of cellulose: the main step of mass loss. *J Anal Appl Pyrolysis* 80:151–165
- Mateyawa S, Xie DF, Truss RW, Halley PJ, Nicholson TM, Shamshina JL, Rogers RD, Boehm MW, McNally T (2013) Effect of the ionic liquid 1-ethyl-3-methylimidazolium acetate on the phase transition of starch: dissolution or gelatinization? *Carbohydr Polym* 94:520–530
- Mazeau K, Heux L (2003) Molecular dynamics simulations of bulk native crystalline and amorphous structures of cellulose. *J Phys Chem B* 107:2394–2403
- Medronho B, Romano A, Miguel MG, Stigsson L, Lindman B (2012) Rationalizing cellulose (in)solubility: reviewing basic physicochemical aspects and role of hydrophobic interactions. *Cellulose* 19:581–587
- Nishino T, Takano K, Nakamae K (1995) Elastic modulus of the crystalline regions of cellulose polymorphs. *J Polym Sci Polym Phys* 33:1647–1651
- Nishiyama Y, Langan P, Chanzy H (2002) Crystal structure and hydrogen-bonding system in cellulose I_β from synchrotron X-ray and neutron fiber diffraction. *J Am Chem Soc* 124:9074–9082
- Paes SS, Sun S, MacNaughtan W, Ibbett R, Ganster J, Foster TJ, Mitchell JR (2010) The glass transition and crystallization of ball milled cellulose. *Cellulose* 17:693–709
- Pinkert A, Marsh KN, Pang SS, Staiger MP (2009) Ionic liquids and their interaction with cellulose. *Chem Rev* 109:6712–6728
- Reddy MM, Vivekanandhan S, Misra M, Bhatia SK, Mohanty AK (2013) Biobased plastics and bionanocomposites: current status and future opportunities. *Prog Polym Sci* 38:1653–1689
- Roig F, Dantras E, Dandurand J, Lacabanne C (2011) Influence of hydrogen bonds on glass transition and dielectric relaxations of cellulose. *J Phys Appl Phys* 44:045403
- Samayam IP, Hanson BL, Langan P, Schall CA (2011) Ionic-liquid induced changes in cellulose structure associated with enhanced biomass hydrolysis. *Biomacromolecules* 12:3091–3098
- Sankri A, Arhaliass A, Dez I, Gaumont AC, Grohens Y, Lourdin D, Pillin I, Rolland-Sabaté A, Leroy E (2010) Thermoplastic starch plasticized by an ionic liquid. *Carbohydr Polym* 82:256–263
- Schneider HA (1989) Glass transition behaviour of compatible polymer blends. *Polymer* 30:771–779
- Schroeter J, Felix F (2005) Melting cellulose. *Cellulose* 12:159–165
- Scott MP, Brazel CS, Benton MG, Mays JW, Holbrey JD, Rogers RD (2002) Application of ionic liquids as plasticizers for poly(methyl methacrylate). *Chem Commun* 1370–1371
- Shi X, Zhang L, Cai J, Cheng G, Zhang H, Li J, Wang X (2011) A facile construction of supramolecular complex from polyaniline and cellulose in aqueous system. *Macromolecules* 44:4565–4568
- Swatloski RP, Spear SK, Holbrey JD, Rogers RD (2002) Dissolution of cellulose with ionic liquids. *J Am Chem Soc* 124:4974–4975
- Szcześniak L, Rachocki A, Tritt-Goc J (2008) Glass transition temperature and thermal decomposition of cellulose powder. *Cellulose* 15:445–451
- Wang H, Gurau G, Rogers RD (2012) Ionic liquid processing of cellulose. *Chem Soc Rev* 41:1519–1537
- Wang QY, Cai J, Zhang LN, Xu M, Cheng H, Han CC, Kuga S, Xiao J, Xiao R (2013) A bioplastic with high strength constructed from a cellulose hydrogel by changing the aggregated structure. *J Mater Chem A* 1:6678–6686
- Yamamuro O, Minamimoto Y, Inamura Y, Hayashi S, Hamaguchi H-O (2006) Heat capacity and glass transition of an ionic liquid 1-butyl-3-methylimidazolium chloride. *Chem Phys Lett* 423:371–375
- Zhang XQ, Wu XL, Gao DC, Xia KN (2012) Bulk cellulose plastic materials from processing cellulose powder using back pressure-equal channel angular pressing. *Carbohydr Polym* 87:2470–2476
- Zograf G, Kontny MJ, Yang AYS, Brenner GS (1984) Surface area and water vapor sorption of macrocrystalline cellulose. *Int J Pharm* 18:99–116